On the UAV based Analysis of Slow Geomorphological Processes: A Case Study at a Solifluction Lobe in the Turtmann Valley

Lasse Klingbeil[1], Erik Heinz[1], Markus Wieland[1], Jana Eichel[2], Thomas Laebe[1], Heiner Kuhlmann[1]

[1] University of Bonn, Institute of Geodesy and Geoinformation, Nussallee 17, 53115 Bonn, Germany, (klingbeil/heinz/wieland/kuhlmann@igg.uni-bonn.de, laebe@ipb.uni-bonn.de)

[2] Karlsruhe Institute of Technology (KIT), Institute of Geography and Geoecology, Kaiserstraße 12, 76131 Karlsruhe, Germany, (jana.eichel@kit.edu)

Key words: Geomorphology, Solifluction Lobe, UAV, Structure From Motion, Terrestrial Laser Scanning, total Station Measurements, Optical Flow, Deformation Analysis

ABSTRACT

In this paper, we investigate the usage of unmanned aerial vehicles (UAV) to assess the geometry and the deformation of a geomorphological phenomenon, which is called a 'solifluction lobe'. Solifluction is the slow downslope movement of soil mass in mountain areas resulting from freeze-thaw processes, which occurs widely in Arctic, Antarctic and Alpine regions. This movement can reach velocities in the order of mm or cm per year. The solifluction lobe under investigation has a size of about 14m x 30m and is located in the Turtmann Valley in the Swiss Alps. We performed two UAV flight campaigns in two consecutive years, generating 3D point clouds and orthomosaics from aerial images using photogrammetric methods. We also recorded a high precision terrestrial laser scan (TLS) in one epoch, which serves as a validation method for the UAV based measurements. Additionally, a number of total station measurements of distinct recognizable points have been performed for validation. We show that in this study it is not possible to discover a deformation of a few centimeters using point cloud comparison methods, as the motion of the lobe is mainly along its surface. However, we were able to detect this motion with an optical flow based method using the orthomosaics. We confirmed this using the total station measurements.

I. INTRODUCTION

Solifluction is the slow downslope movement of soil mass resulting from freeze-thaw processes, which occurs widely in Arctic, Antarctic and Alpine regions (Matsuoka, 2001). Though solifluction movement rates are low with generally mm to cm per year, solifluction is supposed to contribute substantially to sediment transport (Berthling et al., 2002; Matsuoka, 2001). Common landforms created by solifluction processes are tongue-shaped solifluction lobes, which are called "turf-banked" when covered by vegetation. TBL movement rates at the surface vary between 0.3 cm and 21 cm yr^{-1} while subsurface volumetric movement rates range between 0.11 and up to 102 cm^3 yr^{-1} (Matsuoka, 2001). Generally, the 'tread' of the lobe moves more quickly than steep, step-like 'risers' bordering it (Benedict, 1970).

At the surface, solifluction movement is usually measured using tape or point geodetic measurements of markers (e.g. total station surveys, e.) in regular intervals (days to years, e.g. Benedict, 1970). These methods possess several disadvantages, including the low spatial resolution resulting from point measurements and low accuracy and precision due to tilting of pegs downslope in time and operator and measurement errors. Ridefelt et al., (2011) estimated the operator error in their study to range between 0 to 15 mm with an average of 1.5 mm, while the methodological error was estimated to be around 10 mm. In relation to solifluction movement rates in the range of mm to cm, these errors are considerably high.

Only recently, UAV surveying, combined with photogrammetric techniques such as Structure from Motion (SfM), started to be frequently employed in geomorphic research on rivers and hillslopes (Smith et al., 2016; Westoby et al., 2012). However, to our knowledge, so far no one applied UAV and photogrammetric techniques to measure solifluction movement. Although these techniques possess a high potential for this application, there are some challenges inherent to the use case, which are potentially intractable by UAV-based SfM methods.

These challenges are that the signal of interest (the motion of the lobe between the epochs), the expected observation accuracy (relative reconstruction accuracy and registration accuracy between the epochs) and external disturbances (vegetation changes between the epochs) are all in the area of single centimeters. The contribution of this paper is an investigation, if standard structure from motion methods based on aerial images taken with a consumer grade camera, are able to overcome these challenges and to provide useful information about the motion of the solifluction lobe. We do this in the form of a case study in the Turtmann valley, where we quantitatively and qualitatively analyze the results by comparing them with a terrestrial laser scan and total station measurements.

II. Materials and Methods

In this paper we describe several ways to access the geometry of a solifluction lobe in the Turtmann Valley, and its motion between two epochs, which are one year apart. The positions of about 70 nails, which have been driven into the ground of the lobe and the surrounding area are measured using a total station in both epochs, 2014 and 2015. A UAV flight campaign has been performed in both epochs, generating 3D information and orthophotos from aerial images and photogrammetric methods. A high precision TLS scan has been recorded in one epoch (2015). Although the latter cannot be used for deformation analysis, it serves as a validation method for the UAV based measurements. In the following the lobe itself and the various measurement methods are described in detail.

A. *The Lobe*

The investigated turf-banked solifluction lobe is located on the north-exposed, distal slope of a lateral moraine in the Turtmann glacier foreland (Turtmann Valley, Valais, Switzerland) (Figure 1). It possesses a length of 30 m and a maximum width of 14 m (Draebing and Eichel, 2017). The lobe tread, made up by frost-susceptible sandy silt possesses a maximum thickness of 2 m. Soil moisture was found to increase along the lobe tread towards the lobe front, while the coarse material, multistep frontal riser is comparatively dry (Draebing and Eichel, 2017). In addition, the lobe is characterized by closely related geomorphic and ecologic patterns (Eichel et al., 2017). Lobe dimensions are comparatively high for its low age (< 100 years, Draebing and Eichel, 2017), indicating a fast lobe development potentially promoted by vegetation influences (Eichel et al., 2017)

Figure 1: Investigated TBL in the Turtmann Valley with steep risers bordering a flatter lobe tread and UAV flying over the lobe.

B. *Total Station Measurements*

For the investigation of the motion of the solifluction lobe, 70 surveying points were marked on the lobe and the surrounding area (Figure 3). The points were arranged in seven rows crossing the lobe from west to east (i.e orthogonal to the expected direction of motion of the lobe) and measured with a total station in two epochs, 2014 and 2015. In both epochs, the total station was placed at the same station about 75m away from the lobe on bedrock, which is assumed to be stable over both epochs. By using the observations of the total station (slope distance s, horizontal direction r and vertical angle v) the coordinates of the surveying points $\mathbf{p}_{\mathrm{i}}^{(\mathrm{k})}$ were calculated in the local coordinate frame of the instrument for both epochs k (Eq.1) . In addition, the covariance matrix $\mathbf{\Sigma}_{p_i p_i}^{(k)}$ of each point $\mathbf{p}_{\mathrm{i}}^{(\mathrm{k})}$ was calculated via error propagation (Eq.2), where $\mathbf{F}$ denotes the Jacobian matrix of Eq. 1. Due to a tight time schedule the points were measured without repetition and in one face only. Thus, pessimistic values for the accuracy of the observations were chosen: $\sigma_s = 3mm$ and $\sigma_r = \sigma_v = 2mgon$.

$$\mathbf{p}_i^{(k)} = \begin{bmatrix} x \\ y \\ z \end{bmatrix}_i^{(k)} = \begin{bmatrix} s \sin v \sin r \\ s \sin v \cos r \\ s \cos v \end{bmatrix}_i^{(k)} \tag{1}$$

$$\mathbf{\Sigma}_{p_i p_i}^{(k)} = \mathbf{F} \begin{bmatrix} \sigma_{\mathrm{s}}^2 & 0 & 0 \\ 0 & \sigma_{\mathrm{r}}^2 & 0 \\ 0 & 0 & \sigma_{\mathrm{v}}^2 \end{bmatrix} \mathbf{F}^{\mathbf{T}} \tag{2}$$

Since we wanted to avoid additional uncertainty coming from the georeferencing of the total station, we decided to only determine the coordinates of the survey points in the local coordinate frame of the total station and then perform a 6D-Helmert transformation with rotational matrix $\mathbf{R}$ and translation vector $\mathbf{t}$ between both epochs. The residuals of this transformation yield information on the motion of the lobe, assuming that it has not moved uniformly. Five carefully selected points at the corners of the lobe, which were assumed stable over both epochs, were used to estimate the transformation parameters. Following this, the points $\mathbf{p}_i^{2014}$ of the first epoch were transformed and compared to the points $\mathbf{p}_i^{2015}$ of the second epoch. This lead to the residuals $\mathbf{d}$ (Eq.3). The covariance matrix $\mathbf{\Sigma}_{d\ d}^{(k)}$ of the residuals was again calculated via error propagation (Eq. 4), where $\mathbf{J}$ denotes the Jacobian matrix of Eq.3. Here, the accuracy of the points (i.e. $\mathbf{\Sigma}_{p\ p}^{2014}$ and $\mathbf{\Sigma}_{p\ p}^{2015}$) as well as the accuracy of the estimated transformation parameters $\mathbf{\Sigma}_{\boldsymbol{R,t}}$ have to be taken into account.

$$\mathbf{d} = \mathbf{p}^{2015} - (\mathbf{R}\mathbf{p}^{2014} + \mathbf{t}) \tag{3}$$

$$\mathbf{\Sigma}_{d\ d} = \mathbf{J} \begin{bmatrix} \mathbf{\Sigma}_{p\ p}^{2015} & 0 & 0 \\ 0 & \mathbf{\Sigma}_{p\ p}^{2014} & 0 \\ 0 & 0 & \mathbf{\Sigma}_{\boldsymbol{R,t}} \end{bmatrix} \mathbf{J}^{\mathbf{T}} \tag{4}$$

By using a statistic test, it can be analyzed if the residuals $\mathbf{d}$ differ significantly from zero. In this

instance, a point displacement between the two epochs can be verified. The test statistic τ is calculated according to Eq.5 and Fisher distributed with three and infinite degrees of freedom k. The significance level was set to $\alpha = 5\%$ (Heunecke et al, 2013).

$$t = \frac{\mathbf{d}^T \boldsymbol{\Sigma}_{\bar{d}}^{-1}{}_{d} \mathbf{d}_i}{k} \sim F_{k,\infty,1-\alpha} \quad (5)$$

C. *Aerial Images and Structure-from-Motion*

UAV and Camera: In both epochs we performed a flight campaign, using a lightweight UAV (<5kg), which was equipped with a consumer camera. The UAV was custom designed octocopter, based on a Mikrokopter OktoXL construction kit by the company *HiSystems GmbH* (Germany). The camera was a *Panasonic* Lumix GX1 (16 Mpix) with a 20mm fixed focal length lens. The camera was programmed to take images every two seconds, while the UAV was controlled manually in a height of about 10-15m above ground. The reason for the manual flight was the steep incline of the terrain. We wanted a nearly constant height above ground during the flight, and at that time it was not possible to program waypoints for the UAV, which have different heights. One flight covering the whole lobe took about 10 minutes and in each epoch we collected about 400-500 images with a ground resolution of about 4mm. The flight trajectory and the speed was adjusted to reach an overlap of nearly 70-80% along both directions. Although this is somewhat difficult when doing a manual flight, it is necessary for the photogrammetric processing step.

Georeferencing: In order to provide an absolute coordinates system for the derived geometric data, ground control points (GCPs) have been deployed in both epochs (Figure 3).

Figure 2: Tilt & Turn targets used in the 2015 UAV + TLS campaign.

The positions of the GCPs have been determined using a Global Navigation Satellite System (GNSS) receiver in Realtime Kinematic (RTK) operation mode. In the first epoch (2014) we used five printed black and white targets, which were measured with the usual RTK absolute accuracy of a few centimeters. In the second epoch (2015) we used eight tilt&turn targets (Fig.2), which have been originally designed for TLS scan registration. These have been also measured using a RTK GNSS receiver.

We mounted them directly above the ground and tilted them horizontally for the registration of the aerial imagery. We used the same targets tilted vertically to register terrestrial laser scans, which we also performed in the second epochs. This setup allows us to easily compare the UAV and TLS results, since they are tight to the same coordinate system.

Please note, that we use the ground control points to provide a scale to the image based point cloud and the orthophotos and provide an absolute georeference for the presentation and the analysis of the data within a Geoinformation System. We do not use the absolute georeference for the registration of the point clouds and orthophotos of the two epochs.

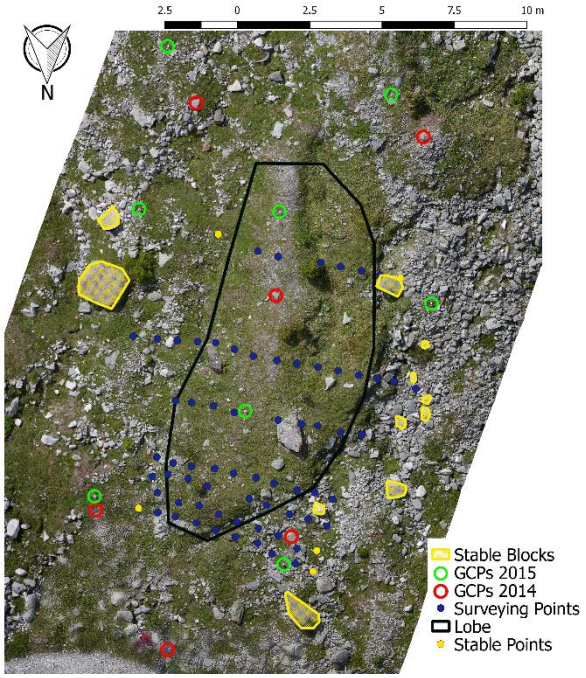

Figure 3: Experimental Setup in 2014 and 2015

Photogrammetric Image Processing We used the software *Photoscan* by the company *Agisoft* (Russia) to determine georeferenced point clouds and orthophotos from the aerial images. This software first aligns the images and estimates a sparse point cloud and the camera poses (position and orientation) in a local coordinate system using a bundle adjustment. This result can be then georeferenced using the GCPs, which are visible in the images. The calibration parameters of the camera have been also estimated as part of this bundle adjustment. In a next step the sparse cloud is

densified using dense image matching methods, which are not further specified by the authors of the software. In this work, we parametrized the software to use the highest possible accuracy for the image alignment and the cloud densification steps and to apply 'mild filtering' during densification. The resulting point clouds are then exported to be analyzed in the open source software *Cloud Compare*.

Agisoft Photoscan was also used for orthophoto generation. The orthophotos provide denser and sometimes visually more accessible information on the surface than the point cloud. They can be used to inspect material properties and vegetation on the lobe (Eichel et al, 2017), and also to estimate motion along the image plane, as this may not be visible from the geometry alone.

Terrestrial Laser Scanning In order to analyze the quality of the point cloud derived from UAV imagery, we additionally generated a point cloud of the lobe in the second epoch using a *Leica ScanStation* P20 terrestrial laser scanner. The object was scanned from five stations. The clouds from the five points were registered and georeferenced using the software *Leica Cyclone* and the tilt&turn targets already described above. In this way, we created a point cloud of the lobe with a resolution of about 5mm, a high relative accuracy (~mm) and an absolute accuracy of a few cm.

D. *Registration and Surface Change Detection*

In order to detect changes between two epochs, the data have to be registered. As we measured the coordinates of the GCPs with RTK GNSS, we expect the absolute accuracy of the point clouds to be in the order of a few centimetres. Given an expected maximal motion of the lobe in the same order of magnitude, we need to use other methods of registering the data (see below). In a second step, the data from two epochs have to be compared in order to determine a change of the surface or more precisely a motion of the lobe. There are several possibilities to measure changes or distances between 3D data, and the most suitable method depends on the type of data. In the described study, we use the following methods.

Total Station Measurements In the case of clearly distinct points in both epochs, these can be directly measured using Total Station measurements as described in 2.B. The registration was realized by the alignment of a number of points, which are assumed stationary over both epochs (Figure 3). The differences are then simply calculated by calculating point-to-point distances.

UAV based point clouds. On order to compare two point clouds, there are several methods (e.g. Barnhart, 2013; Holst, 2017), such as (a) the cloud-to-cloud comparison, where for each point in one cloud the distance to the nearest neighbour in the other is cloud calculated, (b) the cloud-to-mesh comparison, where one cloud is triangulated first, and then for each point of the other cloud its orthogonal distances to the nearest triangle is calculated. We use a cloud-to-mesh approach for comparing UAV point clouds from two epochs and we used the 2014 cloud, which has a higher density, as reference cloud and basis for the mesh. We registered the clouds using areas assumed stationary during both epochs. Here, we selected large stone blocks outside the lobe (Figure 3) and calculated a transformation between them using the Iterative Closest Point (ICP) algorithm (Besl, 1992). Then, this transformation has been applied to all points in order to register the clouds.

UAV cloud and TLS cloud comparison Although the TLS and UAV clouds are from the same epoch, they also need to be registered. As described above, we realized this by using identical GCPs. We then perform the distance calculation using the cloud-to-mesh approach, with the UAV based cloud forming the mesh, as it is denser and smoother than the TLS cloud.

Optical flow based comparison based on images As an additional option, we also consider the orthophotos as data source for the motion analysis. Given precisely registered orthophotos and distinct points, such as edges of stones or other landmarks, in both images, we could simply calculate the shift between these points to determine 2D motion vectors. Although this is only a 2D information, it is likely the dimension with the highest change in the given problem. If 3D shift vectors are needed, one could easily derive the height difference by looking up the heights in the digital surface models used for orthophoto generation. When creating the orthophotos, we incorporated the horizontal component of the transformation, generated using the large stone blocks during the UAV cloud registration. Therefore, the orthophotos are precisely registered as well. The resolution in both photos has been set to 4mm. We then used the Förstner Operator (Förstner, 1987) to automatically find distinct points in the photo from 2014. Förstner points are quite useful in this case, because they are accurate with an estimated covariance for each point. We only used points with an accuracy better than 0.3 pixels. After that we applied a Lucas-Kanade-Tracker (Lucas, 1981) to find these points in the 2015 data. We removed shifts larger than 10 pixels (4cm) as outliers. As there may be a lot of correctly tracked points which do not represent the actual lobe shift, e.g. vegetation growth or moved stones, a robust method has to be applied to see a common trend. Therefore, we calculated the median displacement of grid cells of 300 pixel x 300 pixel (1.2 m x 1.2 m) size.

III. Results and Discussion

A. *Total Station Measurements*

The results of the investigations are shown in Figure 4, which depicts the horizontal displacements of the surveying points between 2014 and 2015. The largest displacements are in the middle and at the northern end of the lobe having a length of up to 3cm. These displacements were found to be significant using the test statistic in Eq.5. Moreover, a clear trend pointing downhill (northward) is apparent, too. Both direction and magnitude of the displacements fit the motion model of a solifluction lobe.

B. *Quality of the UAV point clouds*

In order to evaluate the quality of the point clouds generated from UAV imagery and their applicability in geomorphological problems of smaller scales, such as the one at hand, we compare them with the point cloud from a Terrestrial Laser Scanner.

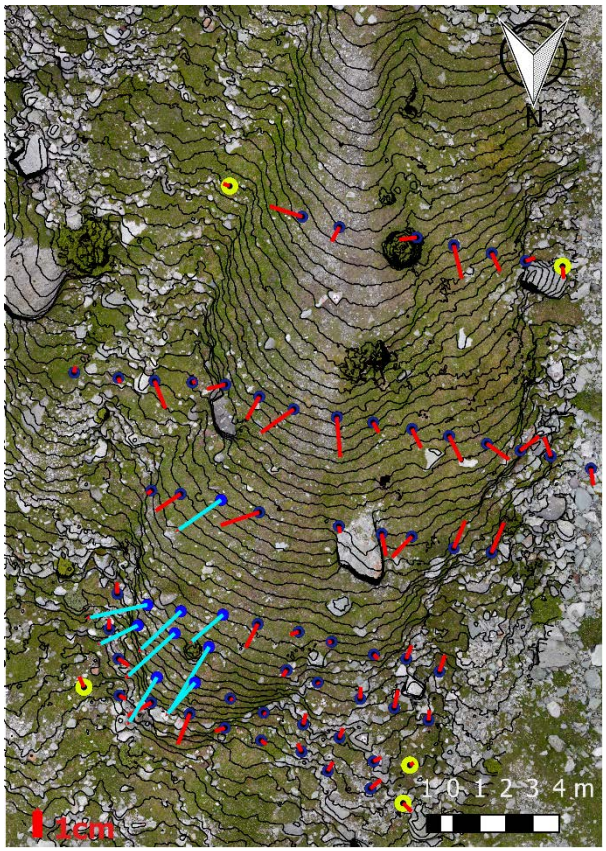

Figure 4: Result of the total station measurements. Arrows show the displacement between both epochs. Blue arrows are significant. The yellow points were used to register both epochs.

During the densification of the point cloud (dense image matching) some assumption are made on the structure of the surface. On the one hand, we expect the resulting point cloud to be a smoothed version of the real surface with small objects being removed as noise or outliers. The smoothing intensity will depend on the settings of the software. On the other hand, we expect the TLS measurement to be more precise with low systematic errors in point cloud generation.

Figure 5 shows a small section of the two point clouds, looking from the side. The round structure, which is visible in the TLS cloud is one of the tilt&turn targets. This target is also visible in the UAV cloud, but in this case it was tilted to be horizontal.

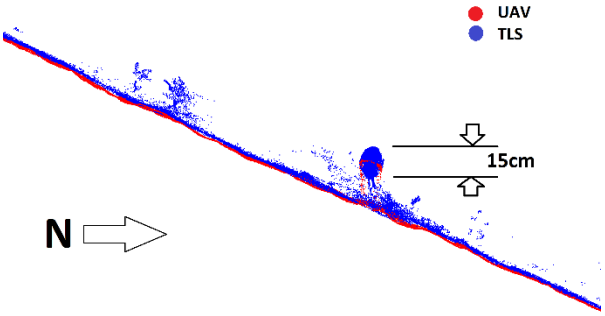

Figure 5: Section of two point clouds on the lobe, viewing from the side (Red: UAV based, Blue: TLS).

Some of the structures, which can be clearly identified as vegetation, are filtered out by the point densification algorithm. The actual surface is reconstructed very similar in both cases, but the UAV cloud seems to have a very small offset, appearing a bit lower than the TLS cloud. This is confirmed in the histogram of all distances and in the map (Figure 6). The offset is in the order of a few millimetres.

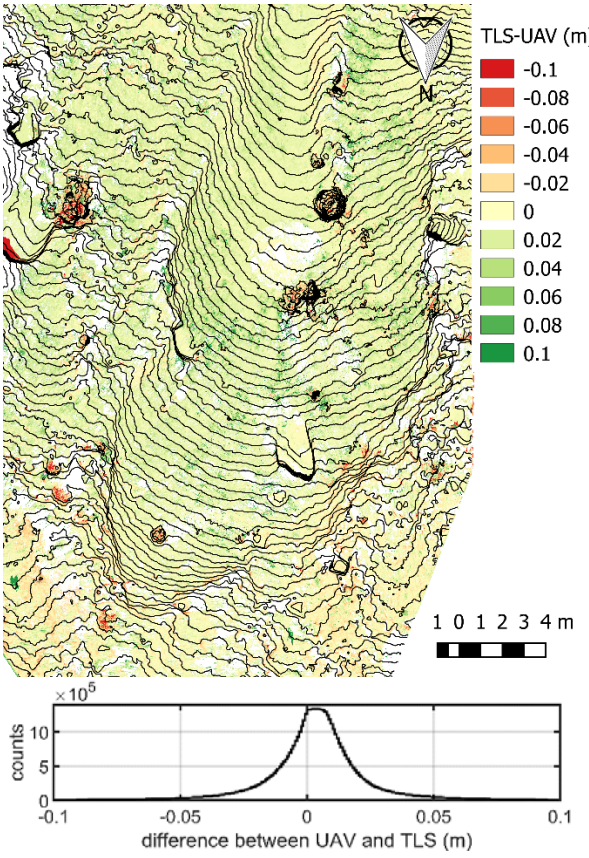

Figure 6: Result of the cloud-to-mesh comparison between TLS and UAV based point clouds. Spatial distribution (top) and histogram (bottom).

In the map, vegetation effects as described above are visible as small darker green patches. Dark red patches, such as the one at the left border of the image, are marking areas, which are not visible in the scan at all due to shadowing effects. It can be summarized, that the point clouds generated from UAV images show an overall accuracy of 1-3cm, when compared to the TLS cloud, which is considered as a reference here. Smaller and more distinct structures are smoothed out due to the photogrammetric reconstruction algorithm. This may also be the reason for the small offset of a few mm, which is visible in Figure 6.

C. *UAV based deformation monitoring*

Point cloud based comparison In order to detect the motion of the lobe based on the UAV imagery we calculated the difference between a triangulated mesh from the 2014 point cloud and the point cloud generated from the 2015 images.

The map in Figure 7 shows the results. There are some smaller structures of darker green and red, which can be identified as changes in vegetation or single stones, which have been moved. There is also a large green area visible at the top of the image above the lobe. As this cannot be explained by any geomorphological process, we assume here an effect resulting from the photogrammetric processing. Reconstructed sections of the point cloud, which are outside of the area of the GCPs, can be subject of distortion or bending of during the image alignment process ('bowl effect'). The area, covered by the the GCPs at the 2015 mission is bigger, and the effect is not existent or smaller in the section, appearing green in the map.

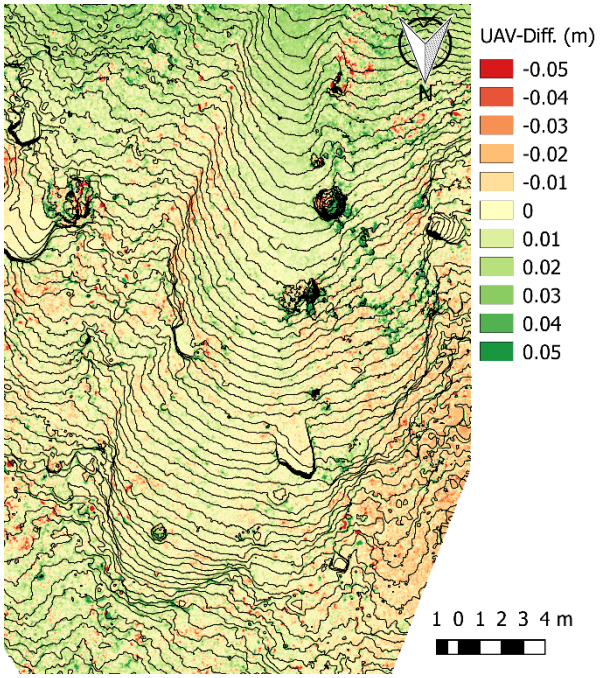

Figure 7: Differences between the two UAV point clouds in 2014 and 2015.

The map in the area of interest does not show any structure, which may be interpreted as a deformation of the lobe. The reason could be there is no or only a very small deformation, or that there is a deformation type, which cannot be detected by the method. In most cases the motion of the lobe would be a motion in the direction of the surface. In a point cloud comparison, where no distinct points can be compared, but rather the form of object, this motion would only visible as differences in the area of the tongue. As the tongue does not show a sharp edge or clear structure, these differences may easily be hidden by vegetation or other more local effects. As a result, even a motion of a few centimetres would not be detectable with sufficient significance with the methods presented so far. Only motions leading to the piling up or flattening of larger areas within the lobe, which show up as significant changes in the vertical direction, would be visible. Apparently these are not present in this case.

Orthophoto based comparison By identifying distinct points in the orthophotos and comparing their position in the image between both epochs, we were able to measure their displacement in the horizontal plane (the plane of the orthographic projection). As described in II.D, we did this using the Förstner-Operator and the Lukas-Kanade-Tracker. The results are shown in Figure 8.

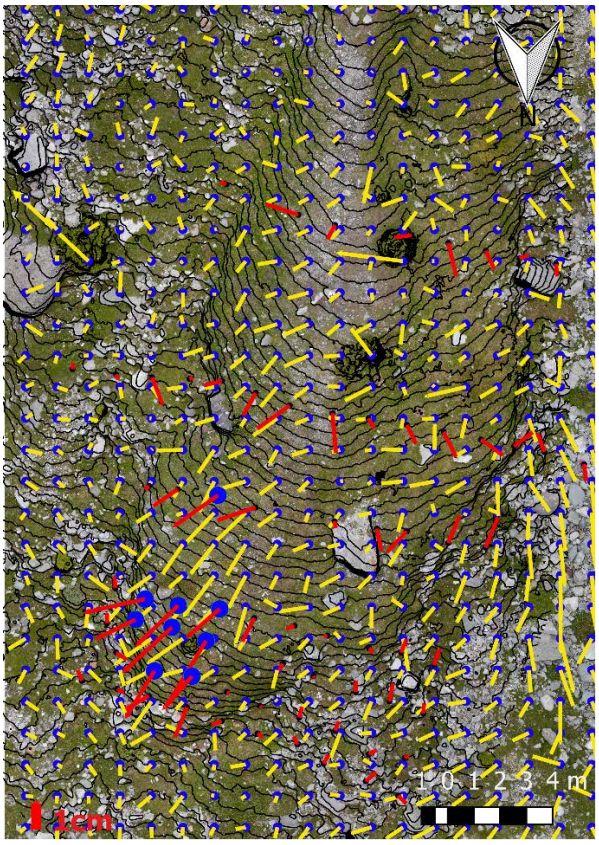

Figure 8: Displacement vectors measured with the total station (red) and using the optical flow based method (yellow).

The yellow arrows represent the median of each 1.2m x 1.2m cell of the image (calculated from about 30-50 displacement vectors per cell). The reference values from the Total Station measurements are shown as red arrows, where the ones with the big blue dots are significant as described above.

Even though there are some apparent outliers, we can see some systematic effects, which are confirmed by the reference data. In the area of the tongue, there is a larger number of longer arrows pointing downhill. Areas outside of the lobe contain mainly shorter arrows, except the area at the right border of the image. This area is a steep decline, consisting of small stones, which could actually have been effected by motion of these stones. However, since this area is outside of the lobe and the GCPs, it could be also a result of the point cloud and the orthophoto generation. It has to be mentioned here, that this method, although it shows promising and plausible results, has to be validated systematically in future research. There are a number of potential systematic errors coming from the point cloud and orthophoto generation, the registration, the point detection and tracking, which will affect the appearance of the displacement vectors. In order to determine the significance of these vectors all errors have to be analyzed and considered. Also the vegetation plays a major role here. As this is likely inducing changes in the order of centimeters, we have to assume, that these are equally distributed in all directions within one grid cell. It would be also possible to exclude vegetation pixel from the analysis. In this context, the result can only be seen as an outlook for further developments.

IV. Summary

In this contribution we analysed the potential of UAV based imagery for the analysis of small scale geomorphological processes in the form of a case study, where we determined the motion of a solifluction lobe between two consecutive years. We showed, that a point cloud created from UAV based imagery in general represents the true geometry with an accuracy in the order of a few cm, except for small inhomogeneous structures, which were filtered out by the reconstruction algorithms. We assume a terrestrial laser scan as a reference here. However, depending on the type and the intensity of the motion, it still not possible to detect a deformation using a point cloud comparison, as motion mainly occurs along the surface of the lobe. A motion of the head of the lobe of about 2cm, which has been detected using total station measurements, could not be detected using the UAV point clouds. Automatic searching for distinct points in the orthophotos of both years and comparing them using optical flow method showed promising results, which were consistent with the reference measurement, but further research is needed to confirm this and analyse the accuracy of this method.

Acknowledgements

This work was partly funded by the DFG (Deutsche Forschungsgemeinschaft) under the project number FOR 1505 'Mapping on Demand' and the BIMODAL project (Biogeomorphic dynamics on lateral moraines in the Turtmann glacier foreland, Switzerland; DI 414/22-1). Vehicle access to the Turtmann glacier foreland was kindly granted by the GOUGRA AG. The authors wish to express their gratitude for this.

V. References

Barnhart, T.B., Crosby, B.T. (2013): Comparing two methods of surface change detection on an evolving thermoskarst using high-temporal-frequency terrestrial laser scanning, Selawik River, Alaska. Remote Sensing, 5(6), 2813-2837

Besl, Paul J.; N.D. McKay (1992). "A Method for Registration of 3-D Shapes". IEEE Transactions on Pattern Analysis and Machine Intelligence. Los Alamitos, CA, USA: IEEE Computer Society. 14 (2): 239–256.

Benedict JB. 1970. Downslope Soil Movement in a Colorado Alpine Region: Rates, Processes, and Climatic Significance. Arctic and Alpine Research 2 : 165–226. DOI: 10.2307/1550306

Draebing D, Eichel J. 2017. Spatial Controls of Turf-Banked Solifluction Lobes and Their Role for Paraglacial Adjustment in Glacier Forelands. Permafrost and Periglacial Processes 28 : 446–459. DOI: 10.1002/ppp.1930

Eichel J, Draebing D, Klingbeil L, Wieland M, Eling C, Schmidtlein S, Kuhlmann H, Dikau R. 2017. Solifluction meets vegetation: the role of biogeomorphic feedbacks for turf-banked solifluction lobe development. Earth Surface Processes and Landforms 42: 1623–1635. DOI: 10.1002/esp.4102

Förstner, W.; Gülch, E. (1987): A Fast Operator for Detection and Precise Location of Distict Point, Corners and Centres of Circular Features. In: Proceedings of the ISPRS Conference on Fast Processing of Photogrammetric Data. Interlaken 1987, S. 281-305.

Heunecke, O.; Kuhlmann, H.; Welsch, W.; Eichhorn, A. & Neuner, H.: Auswertung geodätischer Überwachungs-messungen. Wichmann Verlag, 2013

Holst, C., Klingbeil, L., Esser, F., Kuhlmann, H. (2017) Using point cloud comparisons for revealing deformations of natural and artificial objects, 7th International Conference on Engineering Surveying (INGEO), 18-20 October 2017, Lisbon, Portugal

Lucas, B.D.; Kanade, T. (1981). An iterative image registration technique with an application to stereo vision. Proceedings of Imaging Understanding Workshop, pages 121—130

Matsuoka N. 2001. Solifluction rates, processes and landforms: a global review. Earth-Science Reviews 55 : 107–134. DOI: 10.1016/S0012-8252(01)00057-5

Ridefelt H, Boelhouwers J, Etzelmüller B. 2011. Local variations of solifluction activity and environment in the Abisko Mountains, Northern Sweden. Earth Surface Processes and Landforms 36 : 2042–2053. DOI: 10.1002/esp.2225

Smith MW, Carrivick JL, Quincey DJ. 2016. Structure from motion photogrammetry in physical geography. Progress in

Physical Geography: Earth and Environment 40 : 247–275. DOI: 10.1177/0309133315615805

Westoby MJ, Brasington J, Glasser NF, Hambrey MJ, Reynolds JM. 2012. 'Structure-from-Motion' photogrammetry: A low-cost, effective tool for geoscience applications. Geomorphology 179 : 300–314. DOI: 10.1016/j.geomorph.2012.08.021